A FAR RANGE IMAGE PROCESSING METHOD FOR AUTONOMOUS TRACKING OF AN UNCOOPERATIVE TARGET

Heike Benninghoff, Tristan Tzschichholz, Toralf Boge, and Gabriella Gaias

German Aerospace Center (DLR), 82234 Wessling, Germany

ABSTRACT

This paper proposes an image processing method for far range rendezvous. A target spacecraft at distances up to 30 km is tracked from camera images. The method is based on linking bright, connected sets of pixels over sequences of images. Stars and the target spacecraft are identified by using a star catalog and performing motion segmentation. The algorithm is illustrated in detail and results of a flight experiment called ARGON are presented. The experiment took place in the extended phase of the PRISMA mission. The image processing method was employed and a successful rendezvous from 30 km to 3 km was accomplished using optical navigation.

Key words: Image Processing, Tracking, Rendezvous, On-Orbit Servicing.

1. INTRODUCTION

Service missions for satellite lifetime extension and missions to decrease space debris gain increasing focus. In a so-called on-orbit servicing (OOS) mission, a service spacecraft (chaser) approaches a target object (client) in its orbit. After capturing and docking on the target, it performs various service tasks like the takeover of its orbit and attitude control, refueling or removing an inoperative satellite at the end of its lifetime.

The far range rendezvous, starting from large distances (up to 30 km) and ending at a few hundred meters, is of high importance in the first phases of the approach to the target spacecraft. A robust and reliable estimation of the relative position with respect to the target has to be provided by a navigation system. Relative optical navigation can be performed by using a monocular camera as rendezvous sensor. For estimation of the relative position, the concept of angles-only navigation [11] is employed. In this method, the direction to the target (line-of-sight, LOS) is extracted from camera images and serves as measurement for a navigation filter.

In detail, the image processing system first needs to extract the objects of interests, i.e. sets of bright, connected pixels, from the raw sensor data. In a second step, the objects have to be identified as stars, target or camera hotspots. The identification is based on tracking, motion segmentation and use of a star-catalog. In order to determine the direction to the target, i.e. the line-of-sight vector, in an inertial reference system, the service spacecraft's attitude and the attitude of the camera with respect to the satellite has to be known. The attitude information is also a prerequisite to identify stars from a star catalog. Therefore, the spacecraft's attitude needs to be provided to the image processing system. The attitude of the camera can be previously calibrated on-ground. As an alternative, we propose an on-board attitude estimation which compares the position of the stars in the image with the direction to the stars delivered by the star catalog and computes the attitude by solving a least-squares problem.

The image processing algorithm has been tested in a rendezvous experiment called ARGON (Advanced Rendezvous demonstration using GPS and Optical Navigation) [3]. It was conducted by DLR-GSOC in the extended phase of the PRISMA mission. DLR-GSOC could demonstrate far range rendezvous technology based on angles-only navigation and successfully performed an approach from 30 km to 3 km. This paper concludes with the image processing results gained during the ARGON experiment.

2. FAR RANGE IMAGE PROCESSING

The image processing method for far range rendezvous consists of the detection of objects of interest (=clusters), the identification of stars, target and hotspots, which is performed by using a star catalog and by motion-segmentation. The camera attitude and the line-of-sight vector of the target in J2000 coordinate system are computed.

The J2000 coordinate frame is an Earth-centered inertial (ECI) frame whose origin is the Earth's center of mass. The x-axis is aligned with the mean equinox on 1st of January, 2000 at 12:00 terrestrial time. The z-axis points to the north and the y-axis completes the right hand system.

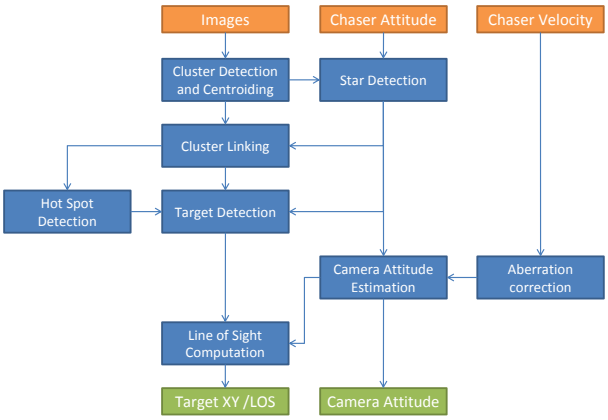

Figure 1. Overview on the Algorithm for Far Range Image Processing

The far range image processing system sequentially processes the images according to the workflow depicted in Fig. 1. There, the single components of the algorithm are presented together with their interactions. Inputs to the system - marked in orange - are the current image, the attitude of the chaser and its velocity. Output - marked in green - consists of the target's position in 2D image coordinates, the line-of-sight vector and the camera's attitude.

2.1. Detection of Objects of Interest

In the first step of the image processing algorithm, all objects of interest should be detected in a given camera image. The objects might be stars, the target or other celestial objects (moon, planets). In addition, camera hotspots can occur. Hot spots or hot pixels are pixels which look much brighter since they do not react proportional to incoming light. The pixels are called hot, as the effect is increasing at high temperature.

Let $I : \Omega \to [0,1]$ be the image intensity function of a given grey-scaled image, where 0 corresponds to black and 1 to white color. Further, $\Omega = [1, N_x] \times [1, N_y]$ is a rectangular image domain and N_x and N_y denote the number of pixels in x- and y-direction.

The objects of interest are also called clusters. A cluster is a set of connected pixels, where each pixel exceeds a threshold $I_1 \in [0,1]$ and at least one pixel exceeds a threshold I_2. The thresholds can be set to constants which are provided in a configuration file, or can be computed automatically based on the dynamic range, the brightness of the background and the brightness of the stars.

The image is scanned pixel-wise. If a pixel's brightness exceeds I_2, a cluster around that pixel is generated. A recursive scheme is applied which marks all pixels in a neighborhood of that pixel to belong to the cluster, if their brightness is greater than I_1. Having determined a set of pixels S which form a cluster, the brightness center is computed by

$$\vec{c} = \frac{\sum_{\vec{p} \in S} I(\vec{p}) \vec{p}}{\sum_{p \in S} I(\vec{p})}. \tag{1}$$

This process is called centroiding. Note, if all pixels had equal intensity, the brightness center would match with the geometric center. For later use, we define the weighted size

$$s = \sum_{\vec{p} \in S} I(\vec{p}). \tag{2}$$

Using the available attitude information of the chaser and a star catalog, some of the clusters can be identified as stars. In a star catalog, e.g. the ESA Hipparcos catalog [8], the direction to a star is given by two angles, right ascension α and declination δ. The line-of-sight vector of the star in J2000 system is related to α and δ by

$$\vec{r}_{\text{star}}^{\,\text{J2000}} = \begin{pmatrix} \sin(\alpha)\cos(\delta) \\ \cos(\alpha)\cos(\delta) \\ \sin(\delta) \end{pmatrix}. \tag{3}$$

It is further transformed to the camera system by

$$\vec{r}_{\text{star}}^{\,\text{cam}} = R_{\text{SC}}^{\text{cam}} R_{\text{J2000}}^{\text{SC}} \vec{r}_{\text{star}}^{\,\text{J2000}}. \tag{4}$$

The transformation matrix from the spacecraft's body frame to the camera reference frame is given either by previous on-ground calibration or can be determined onboard. The latter case is described in detail in section 2.4.

The 2D position of the stars in the image is then computed by applying a camera model, i.e. by computing $h(\vec{r}_{\text{star}}^{\,\text{cam}})$, where $h : \mathbb{R}^3 \to \mathbb{R}^2$ is a function which maps three-dimensional direction vectors to two-dimensional positions in the image. The camera model h makes use of camera parameters like focal length, sensor chip size, image center point and eventual distortion parameters like radial and tangential distortion coefficients.

Only stars which have a positive z-component of $\vec{r}_{\text{star}}^{\,\text{cam}}$ and which lie in the field of view limits of the camera, i.e. which 2D position lies in Ω, are considered. Further, their magnitude which describes its brightness must not exceed a maximum magnitude value. The apparent magnitude of a celestial object, e.g. of a star, measures its brightness observed from Earth. If an object is of 1 magnitude smaller than another one, it appears 2.512 times brighter, cp. [5].

The 2D image position of the remaining stars are compared with those of the previously determined clusters. If a theoretical star position is close to a cluster, the cluster is marked as a star.

2.2. Tracking

In order to identify the target by motion estimation, we need to link clusters from two sequential images. Let $\vec{c}_i^{\,\text{prev}}$ denote the center of a cluster with index i in the

previous image. If the cluster is marked as a star, its position in the current image can be propagated by making use of the attitude change of the chaser.

For that, let t be the time where the previous image has been captured and $t + \Delta t$ the time corresponding to the current image. The attitude of the chaser at time t can be expressed as a rotation matrix $R^{\mathrm{SC}}_{\mathrm{J2000}}(t)$. Let $\vec{r}^{\,\mathrm{cam}}_i(t)$ be the 3D direction vector in the camera system corresponding to the 2D point $\vec{c}^{\,\mathrm{prev}}_i$ in image coordinates. We propagate

$$\vec{r}^{\,\mathrm{J2000}}_i = R^{\mathrm{J2000}}_{\mathrm{SC}}(t) R^{\mathrm{SC}}_{\mathrm{cam}}\, \vec{r}^{\,\mathrm{cam}}_i(t), \tag{5a}$$

$$\vec{r}^{\,\mathrm{cam}}_i(t + \Delta t) = R^{\mathrm{cam}}_{SC} R^{\mathrm{SC}}_{\mathrm{J2000}}(t + \Delta t)\, \vec{r}^{\,\mathrm{J2000}}_i. \tag{5b}$$

Note, that $R^{\mathrm{J2000}}_{\mathrm{SC}}(t) = \left(R^{\mathrm{SC}}_{\mathrm{J2000}}(t)\right)^T$. By applying the camera model, we recompute the image coordinates of $\vec{r}^{\,\mathrm{cam}}_i(t + \Delta t)$, i.e. we set

$$\vec{c}^{\,\mathrm{prop}}_i = h\left(\vec{r}^{\,\mathrm{cam}}_i(t + \Delta t)\right), \tag{6}$$

which is the propagated position of the cluster i for the current image.

Let $\vec{c}_j$ denote a cluster of the current image. The position deviation is defined by

$$\Delta p(i,j) = \begin{cases} \|\vec{c}_j - \vec{c}^{\,\mathrm{prop}}_i\|, & \text{if cluster } i \text{ is a star,} \\ \|\vec{c}_j - \vec{c}^{\,\mathrm{prev}}_i\|, & \text{else,} \end{cases} \tag{7}$$

where $\|.\|$ denotes the Euclidean norm. Let s^{prev}_i denote the weighted size of a cluster i of the previous image, i.e. the sum of the brightness values of the pixels which belong to the cluster. Accordingly, let s_j denote the weighted size of a cluster j of the current image. The size deviation is defined by

$$\Delta s(i,j) = |s_j - s^{\mathrm{prev}}_i|. \tag{8}$$

Using position and size deviation, we define the following similarity measure which describes how good two clusters match:

$$\mu(i,j) = \frac{\omega_p \Delta p(i,j) + \omega_s \Delta s(i,j)}{\omega_p + \omega_s}, \tag{9}$$

where ω_p and ω_s are parameters which weight the position deviation and the size deviation contribution to the similarity measure. In addition, we can make use of thresholds $\Delta p_{\max}$ and $\Delta s_{\max}$. If $\Delta p(i,j) > \Delta p_{\max}$ or if $\Delta s(i,j) > \Delta s_{\max}$, we set $\mu(i,j) = \infty$. Therefore, the pair (i,j) cannot be linked. If the position deviation or the size deviation to all clusters of the previous image exceeds the threshold for a cluster $\vec{c}_j$, it will not be linked to any cluster of the previous image. This occurs typically when new stars emerge close to the boundary of the image.

The linking problem is solved with the Hungarian method, also known as Kuhn-Munkres algorithm. It is a combinatorial optimization algorithm which tries to find a perfect matching with minimum overall costs. Details on the algorithm can be found in [7].

Having linked two clusters, the average velocity of the cluster can be updated. In detail, let $\vec{v}(t) \in \mathbb{R}^2$ be the average velocity of cluster i from the previous image. Let N be the number of previous images to which the cluster can be tracked back. The updated average velocity is set to

$$\vec{v}(t + \Delta t) = \frac{N\vec{v}(t) + (\vec{c}_j - \vec{c}^{\,\mathrm{prev}}_i)/\Delta t}{N + 1}. \tag{10}$$

In order to detect hotspots, we consider the average velocity $\vec{v}$ of the clusters. Hotspots have a velocity of zero and therefore differ from the star motion. Without explicit hot spot detection, hotspots could be falsely assigned as the target. Therefore, it is important to detect hotspots and to exclude them from the list of admissible target candidates: Therefore, if the cluster has a sufficient large history, i.e. if $N > N_{\min}$, and if the norm of the average velocity is smaller than a given tolerance $v_{\min}$, the corresponding pixels in the image are marked as hotspots. Typically, the tolerance value is chosen very small, e.g. $v_{\min} = 0.001$ pixels per second.

It has to be noted that this way of automatic hotspot detection should be treated with care if the servicer's attitude guidance is set to target pointing. In this case, also the target's motion in the image is almost zero. Its center of brightness might be non-constant, as lightning conditions can change during one orbit. It has to be analyzed if the target's velocity is still significant big compared to the velocity of the hotspot, such that an appropriate tolerance $v_{\min}$ can be found. Otherwise, it is not recommended to apply the automatic hotspot detection. Alternatively, a list of hotspot locations, identified by the user, can be provided to the image processing system at the beginning of its execution.

2.3. Target Detection by Motion Segmentation

Let I_{linked} denote the set of indices i, such that a cluster $i \in I_{\mathrm{linked}}$ could have been linked to a cluster $prev(i)$ of the previous image. The norm of the position difference is

$$\Delta p_i := \|\vec{c}_i - \vec{c}^{\,\mathrm{prev}}_{prev(i)}\|. \tag{11}$$

Among all clusters in I_{linked}, the target is the cluster which satisfies the following criteria: First, the target must not be marked as a star or as a hotspot. Secondly, among the remaining clusters, its position deviation differs most from the average position deviation. In detail, the average position deviation is defined as

$$avg(\Delta p) := \frac{\sum_{i \in I_{\mathrm{linked}}} \Delta p_i}{\sum_{i \in I_{\mathrm{linked}}} 1}. \tag{12}$$

Let I_{cand} be the set of admissible target candidates, i.e. clusters of I_{linked} which are neither stars nor hotspots. Then, the third criteria can be written as

$$\max_{i \in I_{\mathrm{cand}}} |\Delta p_i - avg(\Delta p)|. \tag{13}$$

2.4. Attitude and Line-of-Sight Estimation

In addition to the target's image pixel coordinates, the line-of-sight vector to the target in J2000 reference system should be computed by the image processing unit. The attitude of the service satellite with respect to J2000 system is provided by the satellite's attitude system. The attitude of the camera with respect to the servicer can be provided by previous on-ground calibration. As an option, the far range image processing algorithm can refine an initial guess of the camera's attitude by a star-tracker like attitude estimation technique.

The main idea is to consider the position of the clusters marked as stars in the image and the direction vector of the stars in J2000. A least squares problem has to be solved to compute the transformation matrix from J2000 to the camera system. It has to be noted that the attitude estimation and the star detection functionality (cp. section 2.1) are coupled. The star detection makes use of the most recent camera attitude estimation whereas the camera attitude is refined by using the detected stars of the current image. Therefore, the attitude computation cannot be accomplished without an a-priori knowledge of the inertial attitude of the service satellite and of the orientation of the camera reference system with respect to spacecraft body frame.

In detail, let n be the number of stars in the current image and let $\{\vec{r}_i^{\,\mathrm{cam}}\}_{i=1}^n$ be the direction vectors in the camera system which have already been computed in the cluster detection step. Let $\left\{\vec{r}_i^{\,\mathrm{J2000}}\right\}_{i=1}^n$ be the direction vectors in J2000 system provided by the star catalog. To determine the unknown transformation from J2000 system to the camera system, the following cost function is minimized:

$$J(A) = \sum_{i=1}^{n} \omega_i \left\| \vec{r}_i^{\,\mathrm{cam}} - A\vec{r}_i^{\,\mathrm{J2000}} \right\|^2, \qquad (14)$$

where $\omega_i > 0$ are weights. In the implementation of the algorithm used to achieve the results presented in the sequel, cp. section 4, we use $\omega_i = 1$ for all $i = 1, \ldots, n$. Minimizing $J(A)$ can be rewritten to an eigenvector problem (*q-method*) for the corresponding quaternion, see [10] for more details. By solving the eigenvector problem, the camera's attitude in J2000 is determined. As the attitude of the service spacecraft is known, the cameras attitude w.r.t. servicer is computed by

$$R_{\mathrm{SC}}^{\mathrm{cam}} = R_{\mathrm{J2000}}^{\mathrm{cam}}\, R_{\mathrm{SC}}^{\mathrm{J2000}}. \qquad (15)$$

The procedure described above can only be performed if enough stars could have been detected in the image, i.e. if the number of stars is greater or equal to a minimum number of stars, e.g. $n \geq n_{\min} = 10$. To handle the problem that some images or even a long sequence of images do not have enough stars for computing the camera attitude, a simple filter is implemented. The use of a filter also has a smoothing effect to the raw, noisy measurement.

An initial guess has to be delivered. Let $\vec{q}_{\mathrm{SC}}^{\,\mathrm{cam}}$ be the camera attitude w.r.t. to the spacecraft frame computed in the last time step. Let $\lambda \in (0, 1)$ be the a weighting parameter. If enough stars are visible, the attitude $R_{\mathrm{SC,new}}^{\mathrm{cam}}$ is computed. Let $\vec{q}_{\mathrm{SC,new}}^{\,\mathrm{cam}}$ denote the associated quaternion. The quaternion is updated by

$$\vec{q}_{\mathrm{SC},0}^{\,\mathrm{cam}} = \lambda \vec{q}_{\mathrm{SC}}^{\,\mathrm{cam}} + (1-\lambda)\vec{q}_{\mathrm{SC,new}}^{\,\mathrm{cam}}, \qquad (16a)$$

$$\vec{q}_{\mathrm{SC}}^{\,\mathrm{cam}} = \frac{\vec{q}_{\mathrm{SC},0}^{\,\mathrm{cam}}}{\|\vec{q}_{\mathrm{SC},0}^{\,\mathrm{cam}}\|}. \qquad (16b)$$

By making use of a small $\lambda \in (0, 1)$, the filter is robust to noise. Furthermore, old measurements have decreasing weight as $\lambda < 1$, which can easily be seen if Eq. 16 is recursively applied. Note, that the camera attitude with respect to the service spacecraft is assumed to be constant or to change only slightly with time. Therefore, we do not need any propagation with time and can make use of this simple filter. Let $R_{\mathrm{SC}}^{\mathrm{cam}}$ be the transformation matrix corresponding to the updated quaternion $\vec{q}^{\,\mathrm{cam}}$.

The target line-of-sight is finally computed as follows. Let $\vec{c} \in \Omega$ be the corresponding center of the cluster which is marked as the target. Let $\vec{r}_{\mathrm{target}}^{\,\mathrm{cam}}$ be the corresponding unit direction vector in the camera system such that $\vec{c} = h(\vec{r}_{\mathrm{target}}^{\,\mathrm{cam}})$. Then the line-of-sight in J2000 system is set to

$$\vec{r}_{\mathrm{target}}^{\,\mathrm{J2000}} = R_{\mathrm{SC}}^{\mathrm{J2000}} R_{\mathrm{cam}}^{\mathrm{SC}}\, \vec{r}_{\mathrm{target}}^{\,\mathrm{cam}}. \qquad (17)$$

2.5. Camera Aberration Correction

The direction to the stars observed with a sensor system like a camera slightly differs from the real, geometric direction due to aberration effects. The motion of the Earth around the sun causes an *annual aberration*. In addition, the motion of the spacecraft around the Earth leads to an *orbital aberration* effect, see [9]. In this section, we describe how to compute an aberration correction quaternion.

First, the spacecraft's velocity in the inertial frame has to be determined. The velocity can be expressed as

$$\vec{v}_{\mathrm{SC}} = \vec{v}_{\mathrm{orbital}} + \vec{v}_{\mathrm{annual}}, \qquad (18)$$

which is the sum of the orbital velocity (spacecraft motion around the Earth) and annual velocity (motion of the Earth around the sun). A detailed description is given in [9]. We assume that the orbital velocity $\vec{v}_{\mathrm{orbital}}$ is available on-board. Otherwise, only the effect of the annual aberration can be considered.

The annual velocity is determined as follows: For ease of computation, we use an average speed of $v = 29.782\,\mathrm{km/s}$ for the Earth's velocity when moving around the sun. According to [9], there is only an error of max. 1.66% when using a constant velocity in contrast to the exact, current velocity. The velocity vector is

$$\vec{v}_{\mathrm{annual}} = \begin{pmatrix} -v\sin(\Phi_0) \\ v\cos(\Phi_0)\cos(\beta) \\ v\cos(\Phi_0)\sin(\beta) \end{pmatrix}, \qquad (19)$$

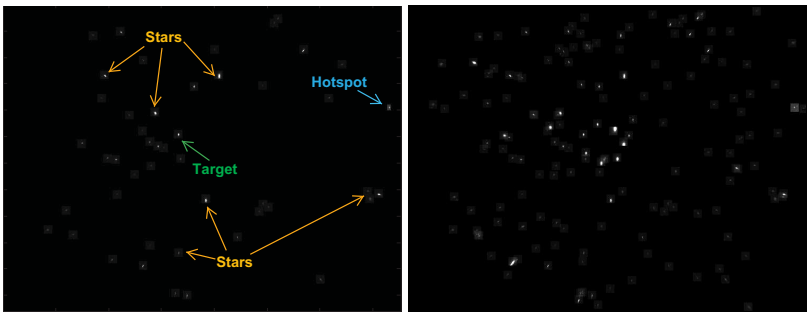

Figure 2. Sample image with target, stars and hotspot (left) taken at April, 25, 2012, 12:18:54 UTC, overlapping of images captured with the far range camera at approx. 16 *km distance (right)*

where $\Phi_0 = 1.75337 + 1.99106\,10^{-7} t_E$ is the so-called sidereal angle in radians and $\beta = 23.439096 \frac{\pi}{180}$ is the angle between ecliptic and equatorial plane in radians. Here, t_E is the time in seconds elapsed since January 1, 2000 at 12:00:00, i.e. it is the GPS time minus 630763213 seconds. Having computed the velocity of the spacecraft, the correction angle can be computed:

The unit vector aligned with the bore sight of the camera head unit in the camera frame is the unit vector in z-direction

$$\vec{r}_{\text{bore}}^{\,\text{cam}} = (0, 0, 1)^T. \tag{20}$$

Transformed to the inertial reference frame

$$\vec{r}_{\text{bore}}^{\,\text{J2000}} = R_{\text{cam}}^{\text{J2000}}\, \vec{r}_{\text{bore}}^{\,\text{cam}}. \tag{21}$$

The correction vector in inertial frame is given by the following cross product:

$$\vec{r}_{\text{cor}}^{\,\text{J2000}} = \vec{v}_{\text{SC}} \times \vec{r}_{\text{bore}}^{\,\text{J2000}}. \tag{22}$$

Performing a back-transformation to the camera system leads to

$$\vec{r}_{\text{cor}}^{\,\text{cam}} = R_{\text{J2000}}^{\text{cam}}\, \vec{r}_{\text{cor}}^{\,\text{J2000}}. \tag{23}$$

The final aberration quaternion is

$$\vec{q}_{\text{abb}} = (\vec{q}, q_w), \tag{24}$$

with $\vec{q} = (q_1, q_2, q_3)^T = 1/(2c)\, \vec{r}_{\text{cor}}^{\,\text{cam}}$, $q_w = \sqrt{1 - q_1^2 - q_2^2 - q_3^2}$, where c is the speed of light.

3. PRISMA-ARGON EXPERIMENT

The DLR/GSOC ground-based rendezvous experiment ARGON (Advanced Rendezvous demonstration using GPS and Optical Navigation) was executed during the extended phase of the PRISMA mission. This experiment is one of the first documented demonstrations of ground-in-the-loop, man-in-the-loop far range rendezvous to a non-cooperative target satellite, see [3, 4]. A successful approach from 30 km to 3 km was accomplished in the time frame April 23-27, 2012. The satellite TANGO played the role of an uncooperative, passive client. The satellite MANGO acted as chaser/servicer. The used sensor

Table 1. Parameters of the VBS far range camera.

Parameter Name	Value	Unit
Resolution	752×580	pixel
Principal point	$(396, 289)$	pixel
Effective focal length	20.187	mm
Size of 1 pixel	$(8.6, 8.3)$	μm
Radial distortion parameter	$(2.6\,\text{e}{-8}, 0, 0)$	

is the Vision Based Sensor (VBS) designed and developed by the Danish Technical University [1], [6]. The VBS instrument is based on an autonomous, high accurate star tracking platform called μASC. For ARGON, the VBS far range camera is only used for collecting images. Fig. 2 shows a sample image, where the target spacecraft, some of the stars and a hotspot are marked (left), and overlapped images captured at a distance of approximately 16 km at during one orbit at 11:30 - 13:00 UTC on April, 25, 2012 (right). The main camera parameters are listed in the Tab. 1, where the radial distortion parameters are taken according to [2].

The VBS Far Range camera performs an on-board preprocessing of the images and automatically extracts so-called regions-of-interests (ROIs). The ROIs are regions around the brightest pixels in the image and are stored in the mass memory of the satellite's on-board computer for later down-link. At each ground contact the following actions where performed on the rendezvous application side [3]: 1) Acquisition of images and telemetry data, 2) determination of the absolute orbit and attitude of the service spacecraft, 3) image processing, 4) relative orbit determination and 5) maneuver planning.

The rendezvous was accomplished fully uncooperative. The available GPS data of TANGO were only used post-facto, to accomplish a GPS precise orbit determination (POD) in order to assess the true performances of the rendezvous.

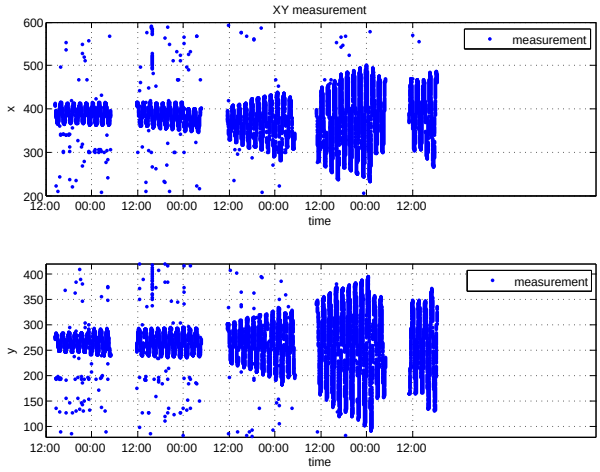

Figure 3. 2D measurement of the target position in the image in pixel coordinates

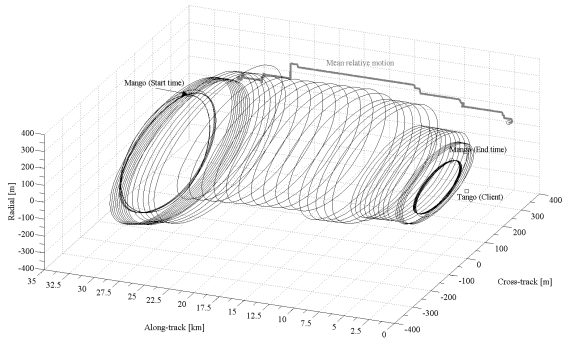

Figure 4. Relative position of MANGO in the relative orbital frame of TANGO [3]

4. RESULTS

The far range image processing algorithm described in this work is based on a previous version of the algorithm which was used for ARGON [3, 4]. This chapter presents the results of the improved image processing algorithm applied on the images captured during the experiment. The main difference compared to the previous version (cp. [3]) is the hit rate of the line of sight measurement. In the improved version, a simple attitude filter is implemented, cp. section 2.4, which provides a continuous attitude estimation, whereas in the previous version a line-of-sight measurement has only been available if enough stars are visible in the image.

Fig. 3 shows the measurement of the target's 2D position in image pixel coordinates. It corresponds to an ellipse-like motion in the image plane, cp. overlapped images at 16 km in Fig. 2 (right sub-figure). The size of the ellipse decreases over the passing of the time. Fig. 4 shows the correspondent actual relative position of MANGO mapped in the orbital frame centered in TANGO. One can note that the mean relative separation spans from 30 km to about 3 km and that the amplitude of the relative orbit is gradually decreasing. Thus, despite the relative orbit is shrunk its trace on the image plane occupies a wider region during the approach. Fig. 3 also shows false target detections (single blue points). For example, if a star cluster is very close to the target, the image of two objects will merge to one cluster. Using the star catalog, this cluster will be assigned as a star and is therefore excluded from the list of admissible target candidates. If there are other clusters, not marked as star or hotspot, one of these clusters will be marked as the target according to the motion segmentation criteria, cp. section 2.3.

Fig. 5 presents the error of the right ascension and declination angle (derived from the line-of-sight vector pointing to the target, cp. Eq. 3) in the camera system. The camera has a field of view of $18.2° \times 13.6°$, which can be computed from the parameters given in Tab. 1. Thus, one pixel error leads to an error of approximately $0.024°$ in the right ascension and declination measurement. The extracted regions of interests (see section 3) are of fixed size. If the target size in the image is large, the preprocessing tends to truncate the target in y-direction. This causes an error in the centroiding and consequently an error in the declination measurement (see Fig. 5) starting from mid of day 3 of the experimental week. There is no remarkable truncation of the target image in x-direction. An example of a nearly correct extraction of a region of interest around the target and an example of a truncated target image is given in Fig. 6.

Tab. 2 shows the hit rate, i.e. the percentage of images where the target has been detected and the accuracy of the right ascension and declination measurement. For the accuracy, 100% refers to all images with a detected target. 16077 images have been processed in total. The target has been detected in 93.86% of the images. In 95.24% of those images, the right ascension could have been determined with an accuracy of 2 pixels, and in 85.53%, the right ascension accuracy is even better than one pixel. The declination could have been determined with a similar accuracy at the first two days where the target image has not been truncated. However, at the last days of the experiment, the declination accuracy decreases. This results in an average percentage of only 44.88% (resp. 63.05%), where a declination accuracy of better than one pixel (resp. two pixels) could have been achieved. The reduced declination accuracy is an effect of this special

Table 2. Hit Rate and Accuracy (in $\%$).

Day	1	2	3	4	5	1-5
Nr Images	1634	2978	3319	5415	2731	16077
Hit Rate	94.92	94.99	92.22	92.63	96.41	93.86
RA err < 0.024	83.50	83.95	85.63	87.30	84.96	85.53
RA err < 0.048	92.33	93.14	95.46	96.31	96.92	95.24
Dec err < 0.024	85.36	85.54	64.62	16.79	07.93	44.88
Dec err < 0.048	91.94	93.21	81.80	40.65	34.49	63.05

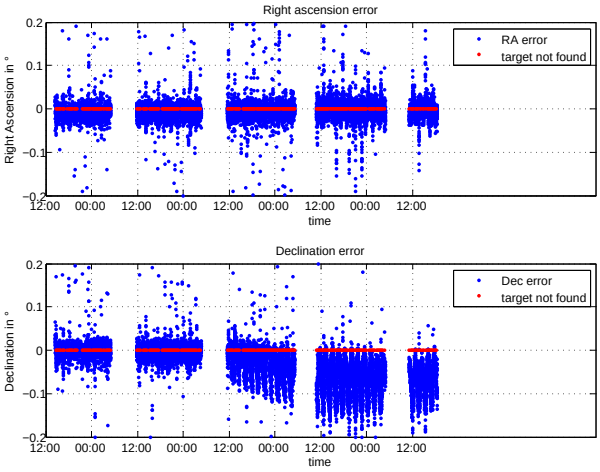

Figure 5. Error in Right Ascension and Declination angle in camera system

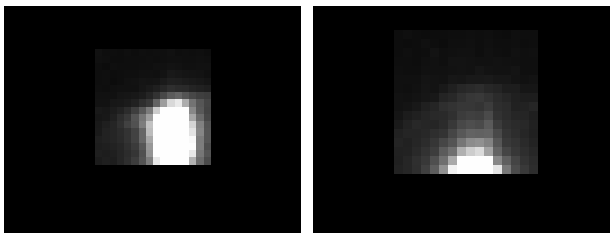

Figure 6. Example of a nearly correct (left) and truncated (right) target image resulting from on-board extraction of regions of interests

type of sensor and preprocessing method. This problem will not occur if the far range algorithm is applied on raw images of other sensors where no previous extraction of ROIs is performed.

Another problem that has to be faced during ARGON is the decrease of visible stars during the experiment. As the target size in the images increases with decreasing distance, the integration time, which is automatically regulated by the camera's shutter control, is reduced such that the target is not over-exposed. As a result, only some of the brightest stars remains visible. Therefore, a significant decrease of the number of detectable stars can be observed, see Fig. 7 which shows the number of detected stars in the images (red) and the mean number of detected stars of 100 images (blue). The on-board camera attitude calibration (cp. section 2.4) is only updated if a sufficient number of stars are visible in the images. In this test of the far range image processing system, the attitude bias is only updated if more than 10 stars have been detected. The result of the camera attitude calibration is presented in Fig. 8. It shows the Euler angles corresponding to the rotation from chaser body frame to camera frame. For Euler angles (ϕ, θ, ψ), the convention '123' is used. The rotation consist of three consecutive rotations: a rotation with angle ϕ around the x-axis, a rotation with angle θ around the resulting y-axis and a rotation with angle ψ around the resulting z-axis.

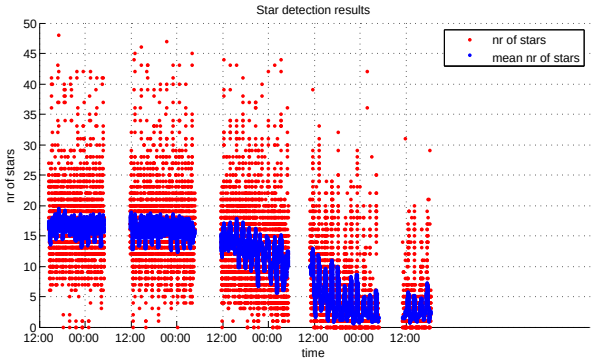

Figure 7. Number of detected stars per image

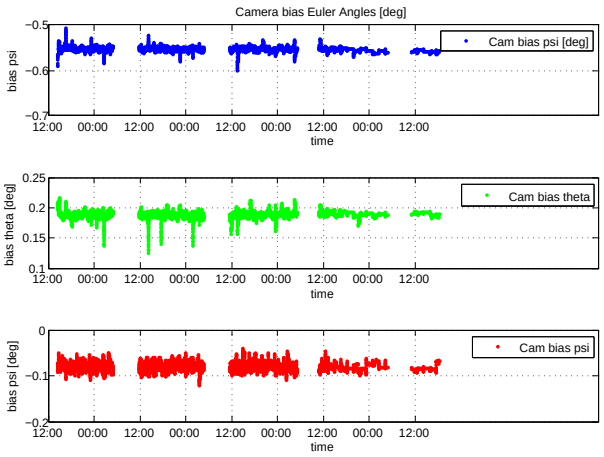

Figure 8. Camera attitude w.r.t. service satellite

The results of the aberration correction, the Euler angles corresponding to $\vec{q}_{\mathrm{abb}}$ (cp. section 2.5), are shown in Fig. 9. The periodicity is a consequence of the orbital aberration effect. The correction mainly affects the pitch angle (2nd component). The maximum correction is ± 0.005 degrees which corresponds to approximately 0.2 pixels. By applying the aberration correction quaternion, the accuracy of the camera's attitude estimation and as a consequence the accuracy of the final target line-of-sight determination can be improved in sub-pixel range. The aberration effect of max. $0.005°$ is smaller than the measurement noise (recall e.g. Fig. 5) but improves the mean error.

During ARGON, the image processing result serves as measurement input for a relative orbit determination system. Fig. 10 reports the relative navigation errors at the estimations times during ARGON. Here, the output product of the GPS precise orbit determination process is taken as reference. The accuracy in the plane perpendicular to the orbital velocity is better because the orbital velocity vector is (approximately) aligned to the bore-sight of the camera. The errors gained at the end of the 26th of April are greater than the average due to the reduction of the number of detected stars and to the begin of the truncation phenomena.

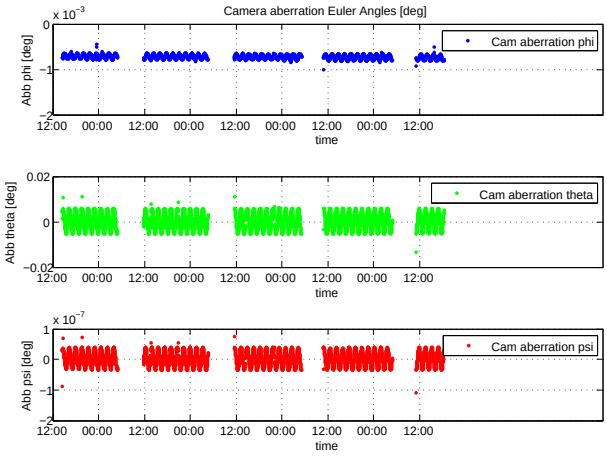

Figure 9. Aberration correction angles

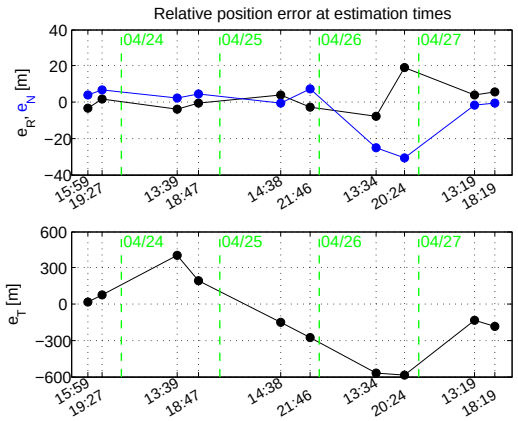

Figure 10. Relative navigation errors, top: error in radial e_{R} and normal direction e_{N}, bottom: error in tangential direction e_{T}

5. CONCLUSION AND OUTLOOK

This paper presented the development of an image processing algorithm for far range rendezvous. The method sequentially tracks a target cluster in a set of images and computes the line-of-sight vector to the target in J2000 inertial system which can be used for a successive navigation. Furthermore, the algorithm includes the option of on-board calibration of the camera's orientation with respect to the service satellite. The far range image processing has been applied and tested during the experiment ARGON, where an approach from 30 km to 3 km has been successfully demonstrated. In the future, the developed image processing can be used for several far range rendezvous scenarios. Visibility of the target and the stars are preconditions for the image processing algorithm to work. Work on radiometric visibility analysis has therefore been started to derive requirements for the camera like necessary integration time, field of view, etc., such that visibility is theoretically guaranteed. Research activities and development in this area are ongoing.

REFERENCES

1. M. Benn. *Vision Based Navigation Sensors for Spacecraft Rendezvous and Docking*. PhD thesis, Danish Technical University (DTU), 2010.

2. M. Benn and T. Denver. Advanced Stellar Compass - Lens Distortion Correction Method for the μASC. *ASC-DTU-MA-3013, Issue 1.0*, 2012.

3. S. D'Amico, J.-S. Ardaens, G. Gaias, H. Benninghoff, B. Schlepp, and J. L. Jørgensen. Non-Cooperative Rendezvous using Angles-only Optical Navigation: System Design and Flight Results. *accepted for publication in Journal of Guidance, Control, and Dynamics*, 2013.

4. S. D'Amico, J.-S. Ardaens, G. Gaias, B. Schlepp, H. Benninghoff, T. Tzschichholz, T. Karlsson, and J. L. Jørgensen. Flight Demonstration of Non-Cooperative Rendezvous using Optical Navigation. In *Proc. 23rd International Symposium of Space Flight Dynamics*, Pasadena, CA, USA, 2012.

5. D. Jones. Norman Pogson and the definition of stellar magnitude. *Astronomical Society of the Pacific Leaflets*, 10(469), 1967.

6. J. L. Jørgensen and M. Benn. VBS - The Optical Rendezvous and Docking Sensor for PRISMA. *Nordic Space*, pages 16–19, 2010.

7. H. W. Kuhn. The Hungarian Method for the Assignment Problem. *Naval. Res. Logist. Quart*, pages 83–97, 1955.

8. M. A. C. Perryman, L. Lindegren, J. Kovalevsky, E. Hoeg, U. Bastian, P. L. Bernacca, M. Creze, F. Donati, M. Grenon, M. Grewing, F. van Leeuwen,

H. van der Marel, F. Mignard, C. A. Murray, R. S. Le Poole, H. Schrijver, C. Turon, F. Arenou, M. Froeschle, C. S. Petersen. The HIPPARCOS Catalogue. *Astronomy and Astrophysics*, 323, 1997.

9. GFZ Potsdam. CHAMP Attitude Aberration Correction. *CH-GFZ-TN-2702, Technical Note*, 2001.

10. J. R. Wertz. *Attitude Determination and Control*. Kluwer Academic Publishers, Dordrecht, Boston, London, 2002.

11. D. C. Woffinden and D. K. Geller. Relative Angles-Only Navigation and Pose Estimation for Autonomous Orbital Rendezvous. *Journal of Guidance, Control, and Dynamics*, 30, 2007.